3-Cell Network MIMO Architectures with Sectorization and Fractional Frequency Reuse

Li-Chun Wang, *Fellow, IEEE*, and Chu-Jung Yeh, *Student Member, IEEE*

***Abstract*—In this paper, we present a 3-cell network multiple-input multiple-output (MIMO) architecture with fractional frequency frequency (FFR) and a novel tri-sector frequency partition scheme. One fundamental question to apply the network MIMO technique in such a high interference environment is: how many base stations should be coordinated together to provide sufficient performance? We will demonstrate that the FFR-based 3-cell network MIMO architecture with the proposed tri-sector frequency partition can not only effectively overcome the inter-group interference, but can avoid executing the complex multi-base-station joint processing for a huge number of cluster of cells at all locations. It will be shown that the proposed 3-cell network MIMO with the rearranged tri-sector frequency partition strategy can outperform the 7-cell network MIMO with omni-directional antennas. Various sector antenna architectures and the method for determining the inner region of the FFR cell planning are also discussed and analyzed on top of the network MIMO system. We hope that this study can provide important insights into the design of the network MIMO systems from the perspectives of architecture and deployment.**

***Index Terms*—network MIMO, fractional frequency reuse, interference cancellation.**

I. Introduction

NETWORK multiple-input multiple-output (MIMO) transmission becomes a hot topic in both industry and academia recently [1]–[7]. It is called the coordinated multi-point (CoMP) transmission in the third Generation Partnership Project (3GPP) Long-Term Evolution-Advanced (LTE-A) and the collaborative MIMO (Co-MIMO) transmission in the IEEE 802.16m Worldwide Interoperability for Microwave Access (WiMAX), respectively [1]–[3]. Network MIMO transmission aims to mitigate the inter-cell interference by coordinating the transmission of a few geographically separated base stations (BSs), but requires reliable high-speed backhaul connections and high computational complexity [4]–[7]. With synchronized BSs, the inter-cell interference in a multi-cell network MIMO system can be mitigated by applying the joint transmission techniques of the multi-user MIMO broadcast systems [8]–[11].

Other widely-used inter-cell interference mitigation techniques are frequency reuse and fractional frequency reuse (FFR). The former scheme avoids utilizing the same frequencies in the neighboring cells, while the latter scheme allows universal frequency reuse for cell-center users. Conventional frequency reuse scheme yields lower spectrum utilization due to fewer available channels in each cell. To reduce the impact of frequency reuse on the throughput for each BS, the FFR scheme (or called reuse partition) assigns a larger frequency reuse factor for the cell-edge users and a smaller frequency reuse factor for the cell-center users. In the code division multiple access (CDMA) based third generation wireless systems, the inter-cell interference issue can be avoided by orthogonal code sequences. Furthermore, a micro-cell deployed CDMA system can increase system capacity than a conventional macro-cell CDMA system [12]. Because the inter-cell interference problem in the orthogonal frequency division multiple access (OFDMA) multi-cellular systems is more serious than that in the CDMA systems, FFR once again becomes an important option for the next generation OFDMA broadband cellular mobile systems [13].

Clearly, combining the network MIMO and FFR techniques can have the advantages of complexity reduction and throughput enhancement. The joint FFR-based network MIMO system can execute the multi-BS joint transmission only for the cell-edge users, and can apply the simple distance separation method for the cell-center users. Thus, the FFR-based network MIMO system can provide the sufficient signal-to-interference-plus noise ratio (SINR) performance and avoid executing the joint multi-BS transmission at all time. Additionally, the universal frequency reuse for the cell-center users can improve the throughput due to higher trunking efficiency of the assigned channels. That is, the geographical locations of cells as well as mobiles now become another degree of freedom that can be exploited for improving the performance of wireless systems. However, the study of network MIMO techniques on top of the FFR cellular system is rarely seen in the literature. Although both FFR and multi-BS joint transmission are possible inter-cell interference cancellation techniques considered in the 3GPP LTE-A and the IEEE 802.16m WiMAX standards, to our best knowledge, how to effectively integrate network MIMO with FFR is still an open issue.

Another fundamental issue in designing the network MIMO system is the following: how many cells shall be coordinated together to provide sufficient SINR performance. Obviously, it is impractical to coordinate too many cells in a network MIMO system because synchronization among a huge number of cells is of high complexity. In both WiMAX and LTE-A standards, the default number of the neighboring BSs for the

Manuscript received June 8, 2010; revised December 4, 2010. This work had been presented in part at the IEEE International Conference on Communications (ICC), Cape Town, South Africa, May 23-27, 2010. This work is sponsored by the National Science Council of Taiwan under grants NSC 99-2221-E-009-026-MY3, and by the Ministry of Education of Taiwan under the MoE ATU Program.

The authors are with the Department of Electrical Engineering, and the Institute of Communications Engineering, National Chiao Tung University, Taiwan (email: lichun@cc.nctu.edu.tw).

Digital Object Identifier 10.1109/JSAC.2011.110607.

joint MIMO processing is three [1], [3], [14], [15]. Even if the number of the coordinated cells of the network MIMO system increases, a group of coordinated cells in network MIMO systems are still affected by the co-channel interference from the neighboring coordinated groups. This kind of the inter-group interference (IGI) should be taken into account when evaluating the performance of network MIMO systems [14], [15]. Hence, it becomes crucial to design a network MIMO system subject to the constraints of three coordinated cells per group and the IGI effects simultaneously.

The ultimate goal of this paper is to investigate which kind of 3-cell FFR-based network MIMO architectures are feasible and can significantly improve SINR performance and capacity subject to the IGI effects. In this paper, we propose a 3-cell FFR-based tri-sector network MIMO architecture with a sector-frequency rearrangement scheme. Specifically, the proposed sector-frequency rearrangement schemes can amplify the performance gain of the network MIMO even with a small number of coordinated cells, i.e., the 3-cell network MIMO case. We examine various tri-sector architectures [16], [17] and determine which directional antenna scheme can effectively reduce the impact of IGI in the multi-cellular system and design the sector frequency rearrangement scheme similar to [18] for the 3-cell network MIMO architecture. Furthermore, we discuss how to determine the uncoordinated inner region for the tri-sector network MIMO with FFR cell planning.

The rest of this paper is organized as follows. In Section II, we discusse the related work for network MIMO and FFR techniques. Section III defines the system model. In Section IV, we briefly review the concept of network MIMO. Section V shows the IGI issue for network MIMO systems. In Section VI, we present the proposed 3-cell network MIMO architecture with FFR. In Section VII, we show numerical results and discuss the inner region issue in Section VIII. We finally give concluding remarks in Section IX.

II. Related Work

In the literature, the related work for the network MIMO techniques for downlink as well as uplink and the FFR techniques can be summarized as follows.

- For downlink cellular networks, the concept of enhancing downlink capacity of a cellular system by the co-processing at transmitting end in a cellular system was proposed [19]. Also, [20] proposed a distributed multi-cell beamforming and analyzed its the performance based on Wyner's circular array model [21]. The coordinated strategies with grouped interior and edges users based on Wyner's circular array model were analyzed in [22]. The authors in [23] compared downlink network MIMO coordination with denser BS deployment. In [24] a block diagonalization scheme was used to form a cluster coordination in a multi-cellular system, including intra- and inter-cluster coordination, to enhance the sum rate and reduce the interference for the cluster-edge users, respectively. In [25], downlink coordination with limited distributed antenna arrays was compared to that with centralized antenna arrays. Under a fixed number of antennas per cell, [26] evaluated the impact of different number of sectors per cell, and the impact of the number of coordinated cells.
- The network MIMO technique has been also studied for the uplink case [27]–[31] . For the uplink network MIMO systems, the coordinated BSs simultaneously receive the multiple users' signals within the area of the coordinated group of cells and suppress the mutual interference between users by means of coherent linear (received) beamforming across BSs. An important issue in uplink network MIMO is which BSs shall be selected for cooperation. The authors in [29] provided dynamic BS clustering approach for uplink BS coordination which resulted in significant sum rate gain compared to the static BS clustering schemes proposed in [30], [31]. Additionally, the issue of how to select a subset of users for jointly coordinated detection to reduce the burden of backhaul was addressed in [27]. It proposed an isolation-based user grouping algorithm to optimize system capacity under a strongly constrained backhaul between seven-coordinated cells, which was also modified to downlink scenario for capacity improvement under a limited backhaul [28].
- The recent researches on FFR were mostly related to the OFDMA systems [32]–[37]. The outage capacity performance of an FFR-based OFDMA cellular system with proportional fair scheduling was studied in [32]. The joint effects of the FFR system parameters, the interior region, and the bandwidth assignment on cell throughput was formulated as an optimization problem in [33]. The resource allocation problem in an FFR-based multi-cell OFDMA system was translated to a graph-coloring problem in [34]. The concept of FFR can be also applied to a tri-sector cellular system [35]. For example, [36] considered the FFR-based tri-sector cellular OFDMA system and showed that the inter-cell interference can be reduced and cell throughput is improved as well by the proposed subcarrier scheduling algorithms. Under similar FFR-based tri-sector cellular OFDMA systems, [37] proposed an interference mitigation scheme by combining partial reuse and soft handover.

III. System Model

We consider a cellular system with $N_{\text{cell}} = 19$ cells, where the center cell has two-tier neighboring cells. In the baseline case, each BS and each user has one single transmit/receive antenna. When the cellular system with three sectors is considered, we assume that each sector is equipped with one sector antenna. The gain pattern used for each sector antenna is specified as [2], [3]

$$A(\theta)_{\text{dB}} = -\min\left[12\left(\frac{\theta}{\theta_{\text{3dB}}}\right)^2, A_m\right], \tag{1}$$

where $A(\theta)_{\text{dB}}$ is the antenna gain at angle θ in decibels and $\theta \in [-180^\circ, 180^\circ]$ is the angle between a mobile user with respect to the main-beam direction of the considered sector antenna. The 3 dB beamwidth θ_{3dB} is the angle of which the antenna gain is 3 dB lower than the antenna gain at the main-beam

direction, and the parameter $A_m = 20$ dB is the maximum attenuation for the sidelobe.

For the transmitted signal x_j from BS j, the received signal of mobile user k is written as

$$y_k = h_{k,j}x_j + \sum_{i\neq j,\, i\in\mathcal{I}} h_{k,i}x_i + n_k \ , \tag{2}$$

where $h_{k,j}$ and n_k are the channel response between mobile k and BS j and the additive noise at the k-th mobile, respectively; and $\mathcal{I}$ is the set of interfering BSs for mobile k. The radio channel models considered in this paper include the effects of Rayleigh fading, shadowing, and path loss. Specifically, we represent the channel response $h_{k,j}$ as

$$h_{k,j} = \alpha_{k,j}\sqrt{\beta_{k,j}\, A(\theta_{k,j})\left(\frac{d_{k,j}}{d_{\text{ref}}}\right)^{-\mu}} \ , \tag{3}$$

where $\alpha_{k,j}$ and $\beta_{k,j}$ are the fast Rayleigh fading and shadowing between mobile k and BS j, respectively; $d_{k,j}$ and d_{ref} are the distance between mobile k and BS j and a reference distance between the center and the vertex of a cell, respectively; and μ is the path loss exponent. $A(\theta_{k,j})$ is the antenna gain for mobile k with respect to BS j whose value is a function of $\theta_{k,j}$ based on (1) for the sectorized antenna and $A(\theta_{k,j}) = 1$ for the omni-directional antenna.

Considering the above signal and radio channel models, we can represent the received signal to noise ratio (SNR) of mobile k from BS j as

$$\text{SNR}_{k,j} = |\alpha_{k,j}|^2\, \beta_{k,j}\, A(\theta_{k,j})\left(\frac{d_{k,j}}{d_{\text{ref}}}\right)^{-\mu}\Gamma \ , \tag{4}$$

where Γ represents the interference-free SNR defined as the SNR measured at the reference distance d_{ref} with only path loss considered, and the noise power is normalized to unity. The parameter Γ captures the effect of various channel and antenna parameters including transmit power, cable loss, transmit and receive antenna heights, thermal noise power, and other link budget parameters. For $d_{\text{ref}} \cong 1.1547$ km, the reference SNR $\Gamma = 18$ dB for a BS-to-BS distance of $R_{\text{B2B}} = 2$ km and a macro-cellular system with 30 Watts' transmit power [38]. For mobile k of BS j, we can express its corresponding SINR as

$$\gamma_{k,j} = \frac{\text{SNR}_{k,j}}{1 + \sum_{i\neq j,\, i\in\mathcal{I}} \text{SNR}_{k,i}} \ . \tag{5}$$

The corresponding channel capacity for each SINR value $\gamma_{k,j}$ can be given by $\log_2(1+\gamma_{k,j})$ bit/s/Hz. In this paper, we consider the achievable capacity for various modulation and coding schemes (MCS) considered in the standard [39]. For the considered MCSs $\{$QPSK$\frac{1}{2}$, QPSK$\frac{3}{4}$, 16-QAM$\frac{1}{2}$, 16-QAM$\frac{3}{4}$, 64-QAM$\frac{2}{3}$, 64-QAM$\frac{3}{4}\}$, the corresponding SINR requirements and the spectrum efficiencies are $\{$6, 8.5, 11.5, 15, 19, 21$\}$ dB and $\{$1.0, 1.5, 2.0, 3.0, 4.0, 4.5$\}$ bit/s/Hz, respectively.

IV. Network MIMO

Network coordination can improve spectral efficiency by eliminating the inter-cell interference in multi-cellular systems [4], [5]. With a high-speed backhaul, the BSs can be synchronized, and all the BSs can exchange the channel state information (CSI) of each coordinated sites via the central coordinator. With full BS cooperation, the downlink network MIMO transmission can be modelled as the downlink transmission in the multi-user MIMO broadcast system. Consider a network MIMO system with M coordinated BSs, each of which transmits data streams to its own target mobile station. Define the transmitted signal vector with M elements as

$$\mathbf{x} = \mathbf{W}\mathbf{s} = \begin{bmatrix} w_{1,1} & \cdots & w_{1,M} \\ \vdots & w_{j,k} & \vdots \\ \underbrace{w_{M,1}}_{\triangleq \mathbf{w}_1} & \cdots & \underbrace{w_{M,M}}_{\triangleq \mathbf{w}_M} \end{bmatrix} \begin{bmatrix} s_1 \\ \vdots \\ s_M \end{bmatrix} \ , \tag{6}$$

where s_k $(k = 1, \ldots, M)$ is the data symbol of the k-th user, and $\mathbf{w}_k$ is the corresponding precoding weight column vector. Note that the j-th antenna output in a network MIMO system is a linear combination of M data symbols, i.e., $x_j = \sum_{k=1}^{M} w_{j,k}s_k$. Then, the users' received signals $\mathbf{y}$ from M BSs are given by

$$\mathbf{y} = \mathbf{H}\mathbf{x} + \mathbf{n} = \begin{bmatrix} \mathbf{h}_1 \\ \vdots \\ \mathbf{h}_M \end{bmatrix}\mathbf{x} + \mathbf{n} \ , \tag{7}$$

where $\mathbf{n}$ denotes the noise vector, $\mathbf{H} = [h_{k,j}]_{M\times M}$ denotes the channel matrix with the channel response $h_{k,j}$ between mobile k and BS j defined in (3), and $\mathbf{h}_k = [h_{k,1}\cdots h_{k,M}]$ is the channel vector of the k-th user. Thus, we can represent the received signals of mobile k as

$$y_k = s_k||\mathbf{h}_k\mathbf{w}_k|| + \sum_{i=1,\, i\neq k}^{M} s_i||\mathbf{h}_k\mathbf{w}_i|| + n_k \ , \tag{8}$$

where $||\mathbf{v}||$ denotes the norm of a vector $\mathbf{v}$.

Denote p_k as the average power of data stream s_k, i.e., $p_k = \text{E}[|s_k|^2]$. According to the network MIMO principle, the following constraint $\text{E}[|x_j|^2] \leq P_{\text{BS}}$ should be satisfied for every BS $j = 1, \ldots, M$. Then, it follows that

$$\begin{bmatrix} |w_{1,1}|^2 & \cdots & |w_{1,M}|^2 \\ \vdots & \ddots & \vdots \\ |w_{M,1}|^2 & \cdots & |w_{M,M}|^2 \end{bmatrix}\begin{bmatrix} p_1 \\ \vdots \\ p_M \end{bmatrix} \leq P_{\text{BS}}\mathbf{1}_M \ , \tag{9}$$

where P_{BS} is the maximum transmit power of each BS, and $\mathbf{1}_M$ is an $M \times 1$ vector with all elements equals one. It is well known that dirty paper coding (DPC) [8] can achieve the capacity of the multi-user MIMO broadcast system. Due to high complexity, suboptimal zero-forcing (ZF) and zero-forcing dirty paper coding (ZF-DPC) multi-user MIMO algorithms were proposed [9]. Similarly, there exist the optimal DPC network MIMO algorithm and the suboptimal ZF and ZF-DPC network MIMO algorithms [5], [6]. We will consider ZF and ZF-DPC network MIMO algorithms in this paper.

A. ZF Network MIMO Transmission

The goal of ZF network MIMO transmission is to invert the channel to obtain $\mathbf{H}\mathbf{W} = \mathbf{I}_M$, where $\mathbf{I}_M$ is an $M \times M$ identity matrix. The weight matrix $\mathbf{W}$ can be obtained by

using the pseudo-inverse of the channel matrix. The received signal vector is hence given by

$$\mathbf{Y} = \mathbf{H}\mathbf{x} + \mathbf{n} = \mathbf{H}\mathbf{W}\mathbf{s} + \mathbf{n} = \mathbf{s} + \mathbf{n} \ . \tag{10}$$

With per-base power constraint (9), the objective of the network MIMO system is to maximize the minimum rate among the coordinated cells, and the corresponding maximum common rate solutions are [5]

$$p_k = \frac{P_{\text{BS}}}{\max\limits_j [\mathbf{W}\mathbf{W}^*]_{(j,j)}} = \frac{P_{\text{BS}}}{\max\limits_j \sum\limits_k |w_{j,k}|^2} \ , \quad \text{for all} \quad k \ , \tag{11}$$

which results in an equal symbol power transmission and $(\cdot)^*$ denotes the conjugate transpose operation. Therefore, the corresponding mobile's rate is given by $\log_2(1 + p_k/\sigma^2)$ bit/s/Hz among all the coordinated cells, where σ^2 represents the noise power. From (11), we can observe that the actual average power of data stream s_k^2 (i.e., p_k), will be lower than the original available transmission power P_{BS} due to beamforming weights.

B. ZF-DPC Network MIMO Transmission

The ZF-DPC network MIMO transmission constructs the linear weight matrix $\mathbf{W} = \mathbf{Q}^*$ through the QR decomposition of the channel matrix $\mathbf{H} = \mathbf{L}\mathbf{Q}$, where $\mathbf{L}$ is a lower triangular matrix with (k, i)-th entry $L_{k,i}$ and $\mathbf{Q}$ is a unitary matrix with $\mathbf{Q}\mathbf{Q}^* = \mathbf{Q}^*\mathbf{Q} = \mathbf{I}_M$. The received signal is written as

$$\mathbf{Y} = \mathbf{H}\mathbf{x} + \mathbf{n} = \mathbf{L}\mathbf{Q}\mathbf{Q}^*\mathbf{s} + \mathbf{n} = \mathbf{L}\mathbf{s} + \mathbf{n} \ , \tag{12}$$

and the corresponding k-th mobile's received signal is $y_k = L_{k,k}s_k + \sum\limits_{i<k} L_{k,i}s_i + n_k$. Note that the weight matrix $\mathbf{W} = \mathbf{Q}^*$ ensures no interference from data symbols with indices $i > k$. The remaining interference from data symbols $i < k$ are taken care of by the successive interference cancellation of DPC. Based on the result of ZF network MIMO transmission, if we set $p_k = p$ for all k, the per-site power constraint (9) becomes $\text{E}[|x_j|^2] = [\mathbf{W}\mathbf{W}^*]_{(j,j)}p = \sum_k |w_{j,k}|^2 p \le P_{\text{BS}}$ for all transmitted signal x_j. Recall that the weight matrix $\mathbf{W} = \mathbf{Q}^*$. We have $[\mathbf{W}\mathbf{W}^*]_{(j,j)} = [\mathbf{Q}^*\mathbf{Q}]_{(j,j)} = [\mathbf{I}_M]_{(j,j)} = 1$. Thus, we can set $p_k = P_{\text{BS}}$ for each coordinated BS. Given the received signal in (12), mobile k can achieve the capacity $\log_2(1+|L_{k,k}|^2 p_k/\sigma^2)$ bit/s/Hz. Note that the channel vectors of channel matrix $\mathbf{H}$ need to reorder similar to the case in traditional multi-user MIMO broadcast systems [40].

V. Effects of Inter-Group Interference on Network MIMO Systems

A. SINR Performance Model

When applying network MIMO in a multi-cellular environment, it is important to include the effects of IGI among the coordinated network MIMO groups. Clearly, a group of coordinated cells will cause interference to the neighboring coordinated group of cells even if the intra-group interference has been cancelled by the joint multi-BS processing. Consider a cell with two-tier surrounding cells layout under M-cell network MIMO coordination. Denote $\mathcal{I}_G$ as the set of index for the interfering network MIMO groups and G_i as the cluster of cells for group i, $i \in \mathcal{I}_G$. Let $[w_{a,b}^{(G_i)}]_{M\times M}$ be the precoding weights for cell $a \in G_i$ with respect to mobile $b = 1, \cdots, M$. With data symbol $s_b^{(G_i)}$ of mobile b, the output signal transmitted from cell a can be represented as

$$x_a^{(G_i)} = \sum_{b=1}^{M} w_{a,b}^{(G_i)} s_b^{(G_i)} \ . \tag{13}$$

From (8) and (13), we can obtain the SINR of mobile k as follows:

$$\gamma_k^{\text{IGI}} = \frac{p_k ||\mathbf{h}_k \mathbf{w}_k||^2}{1 + \sum\limits_{i\in\mathcal{I}_G} \sum\limits_{a\in G_i} \sum\limits_{b=1}^{M} p_b^{(G_i)} |h_{k,a}^{(G_i)} w_{a,b}^{(G_i)}|^2} \ , \tag{14}$$

where $p_k = \text{E}[|s_k|^2]$ and $p_b^{(G_i)}$ are the average power of stream s_k and $s_b^{(G_i)}$, respectively; and $h_{k,a}^{(G_i)}$ is the channel response between the considered mobile k and the interfering BS $a \in G_i$. According to (11) $p_b^{(G_i)} = p^{(G_i)}$. From (14), we can obtain the SINR with ZF-based network MIMO transmission as

$$\gamma_{k,\text{ZF}}^{\text{IGI}} = \frac{p_k}{1 + \sum\limits_{i\in\mathcal{I}_G} \sum\limits_{a\in G_i} \sum\limits_{b=1}^{M} p^{(G_i)} |h_{k,a}^{(G_i)} w_{a,b}^{(G_i)}|^2} \ . \tag{15}$$

If ZF-DPC network MIMO transmission is adopted, the corresponding SINR is represented as

$$\gamma_{k,\text{ZFDPC}}^{\text{IGI}} = \frac{P_{\text{BS}} |L_{k,k}|^2}{1 + \sum\limits_{i\in\mathcal{I}_G} \sum\limits_{a\in G_i} \sum\limits_{b=1}^{M} P_{\text{BS}} |h_{k,a}^{(G_i)} w_{a,b}^{(G_i)}|^2} \ , \tag{16}$$

where $L_{k,k}$ is defined in (12).

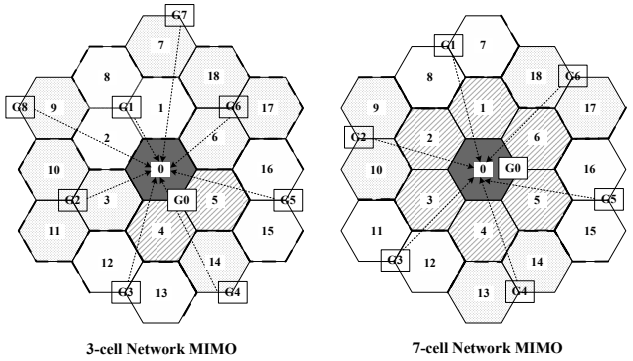

Fig. 1. An example of inter-group interference for the 3-cell and 7-cell network MIMO systems.

B. SINR Performance Degradation

In this section, we explain why IGI affects the performance of network MIMO systems by examples. Fig. 1 shows the 3-cell and 7-cell network MIMO systems. In the case of 3-cell network MIMO, cells 0, 4 and 5 forms a 3-cell network MIMO group G_0. Although for cell 0, network MIMO transmission cancels the intra-group interferences from cells 4 and 5, many two-tier cells still cause interference to cell 0. In this case, $\mathcal{I}_G = \{1, 2, \ldots, 8\}$ and the corresponding cells in each group are $G_1 = \{1, 2, 8\}$, $G_2 = \{3, 10, 11\}$, $G_3 = \{12, 13\}$, $G_4 =$

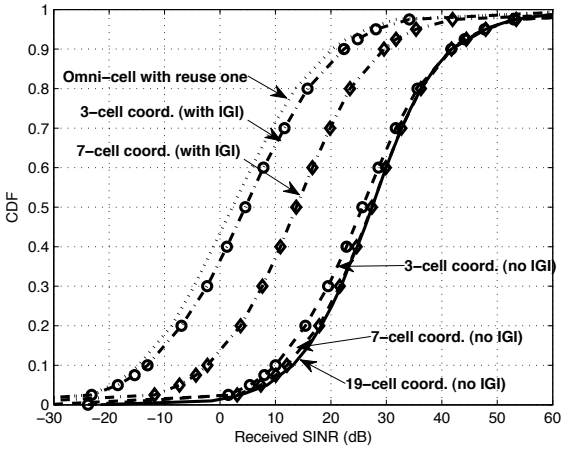

Fig. 2. Effects of inter-group interference for the 3-cell and 7-cell network MIMO systems.

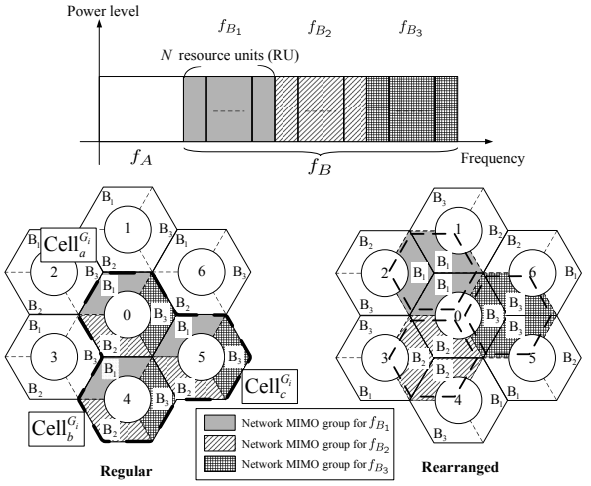

Fig. 3. Fractional frequency reuse (FFR) sectorization for proposed 3-cell network MIMO coordinations.

$\{14\}$, $G_5 = \{15, 16\}$, $G_6 = \{6, 17, 18\}$, $G_7 = \{7\}$, and $G_8 = \{9\}$. After the network MIMO cancelling the inter-cell interference for cell 0, there still exists 4 and 12 first-tier and second-tier interferers, respectively. Note that all the interferers also transmit M-cell coordinated signals. In a 7-cell network MIMO system, the coordinated partners of cell 0 are cells {1, 2, 3, 4, 5, 6}. In this case, the IGI from the second-tier cells 7 to 18 cannot be reduced by the multi-BS joint processing.

Figure 2 shows the effects of IGI on the ZF-DPC network MIMO through 5×10^4 channel realizations. At the 10 % outage probability, the IGI effects degrade the SINR by 14 dB and 23 dB for the 7-cell and 3-cell network MIMO systems, respectively. For comparison, the performances of network MIMO without the IGI effects are also shown in the figure, i.e., 19-cell (solid line), 7-cell (diamond legend), and 3-cell (circle legend). We find that without IGI effects the SINR performance of 7-cell network MIMO system approaches that of the 19-cell network MIMO system. This result implies that the coordination size $M = 7$ is enough for designing network MIMO systems in the case without IGI effects. However, the received signal quality of the network MIMO systems will be deeply affected when interferences from the other groups are considered.

C. Unbalanced Signal Quality Effects

Based on the observation from the 7-cell network MIMO system, the IGI incurs an unbalanced signal quality issue when a large coordination size is used. That is, the central cells among a coordinated group have better signal quality than the edged cells. Take the 7-cell network MIMO as the example. The IGI for cell 0 is from the second-tier interferers as mentioned before. However, the edged cells $\{1, 2, 3, 4, 5, 6\}$ have three first-tier interferers and 15 second-tier interferers. As a result, the edge cells will suffer more serious IGI than the central cells especially when the coordination size M increases. Hence, the signal quality among M coordinated cells is unbalanced in the conventional network MIMO architecture. To sum up, the IGI causes severe performance degradation and the unfairness issue among a group for multi-cellular network MIMO systems.

Note that the 3-cell network MIMO does not suffer from this unbalanced issue because each member in a coordinated group has the same geographic condition. In other words, each cell is an "edged cell" in the 3-cell group and has the same interferers distribution. However, the performance improvement resulted from such a small-size coordination is not significant from Fig. 2. In the following section, we propose a novel network MIMO architecture to improve the signal quality and achieve the fairness among a group of cells simultaneously.

VI. Frequency Partition-based Three-cell Network MIMO

A. FFR with Sectorization

Figure 3 shows the FFR planning for a tri-sector cellular system. In this figure, frequency bands are partitioned into the inner frequency bands f_A and the outer frequency bands f_B, where f_B is further partitioned into three subbands f_{B_1}, f_{B_2}, and f_{B_3} (the gray, slash, and grid area, respectively). In general, the inner frequency bands f_A adopts universal reuse factor one with omni-directional antenna for the interior cell users; the outer frequency bands f_B adopts reuse factor $1/3$ for the users in each sector. By means of FFR, the intra-cell interference can be avoided due to four orthogonal subbands. Assume f_{B_1}, f_{B_2}, and f_{B_3} have the same bandwidth with N frequency resource units (RU) in each outer subband, i.e., $f_{B_p} = \{f_{B_{p,1}}, \ldots, f_{B_{p,N}}\}$ for $p = 1, 2, 3$.

In this paper, we consider two kinds of tri-sector frequency planning methods: regular and rearranged frequency partitions. In the traditional regular tri-sector frequency partition, the sectors with the same main-beam direction at each cell are with the same frequency band (e.g. the left cellular system in Fig. 3), which can be found in [35]–[37]. As for the rearranged tri-sector frequency partition, the sectors with the same main-beam direction at the neighboring cells can have different frequency bands as shown in the right part of Fig. 3. We

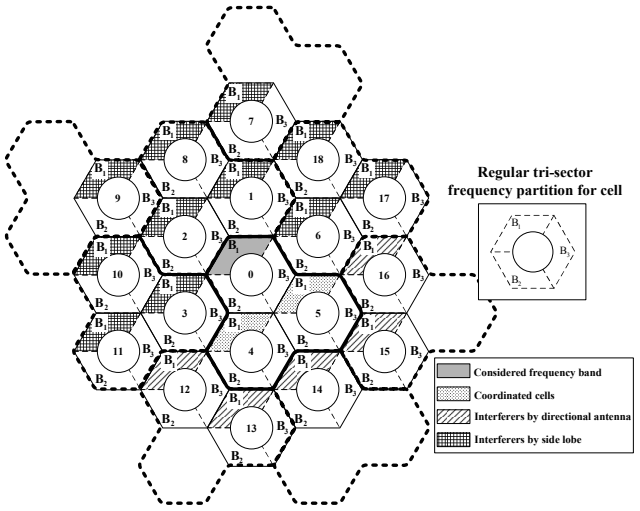

Fig. 4. Interference example for 3-cell FFR-based network MIMO with regular tri-sector frequency partition (consider cell 0).

will design the network MIMO systems based on the above two tri-sector frequency partitions. Although the rearranged tri-sector frequency partition may yield severer co-channel interference than the regular tri-sector frequency partition, we will show that combining the 3-cell network MIMO with the rearranged tri-sector frequency partition can outperform the 3-cell network MIMO with regular tri-sector frequency partition.

B. FFR-based Network MIMO with Regular Tri-Sector Frequency Partition

In this section, we combine network MIMO with FFR and the regular tri-sector frequency partition. As mentioned before, the FFR method partitions the whole frequency band into different zones. Compared to the conventional omni-cell with universal frequency reuse factor of one, the tri-sector cellular system combined with FFR can significantly reduce the interference, while fully utilizing the frequency band at each cell. As an example in Fig. 4, when a user of cell 0 utilizes one of RU $f_{B_{1,n}}$ $(n = 1, \ldots, N)$ in frequency band f_{B_1}, the interference comes from 7 cells {4, 5, 12, 13, 14, 15, 16} under the assumption of perfect 120° sector antenna rather than being interfered by all 18 cells in the omni-directional case. Here, the question is how we can further improve the SINR on top of FFR? The solution proposed in this paper is to further incorporate the network MIMO technique with FFR.

From Fig. 4, we find that the seven interfering sources consists of two critical interferers coming from first-tier neighboring cells 4 and 5 and five weaker second-tier interferers due to higher path loss. Therefore, we use the network MIMO technique to cancel the two most severe interference. Instead of coordinating huge number of cells, we propose a coordination scheme with only three cells. We define those coordinated cells as a group shown in Fig. 3. For the arbitrary group G_i, we label the three cells as $\text{Cell}_a^{G_i}$, $\text{Cell}_b^{G_i}$, and $\text{Cell}_c^{G_i}$, respectively. For the 3-cell coordination, we can apply network MIMO transmission to each subband $f_{B_{p,n}}$ for $p = 1, 2, 3$ and $n = 1, \ldots, N$. Under the assumption of perfect sector directional antenna, the channel matrix of $f_{B_{1,n}}$ for cell 0 in the group $\{0, 4, 5\}$ is

$$\mathbf{H}(f_{B_{1,n}}) = \begin{bmatrix} h_{(0),0} & h_{(0),4} & h_{(0),5} \\ 0 & h_{(4),4} & 0 \\ 0 & 0 & h_{(5),5} \end{bmatrix}, \tag{17}$$

where (x) denotes the corresponding served user in cell x. We eliminate the interference caused by $h_{(0),4}$ and $h_{(0),5}$ (from cells 4 and 5) by network MIMO. As a result, the two most severe interference is cancelled through a small-sized (3×3) matrix computation. Importantly, this small-sized cooperation scheme can be applied to all the cells within the entire service area. For example in Fig. 4, at certain time slot we have many cooperated groups among the 19-cell layout: cells $\{0, 4, 5\}$, $\{8, 2, 1\}$, $\{10, 11, 3\}$, and $\{18, 6, 17\}$. Not only the middle cell (cell 0) is coordinated with its neighboring cells, but the cells in the outer layer are also coordinated simultaneously.

1) Cells Regrouping and Partner Selection: In this section, we propose a cell regrouping and partner selection scheme to address the service fairness issue caused by the network MIMO systems with the regular tri-sector frequency partition. From Fig. 4, among arbitrary group G_i, the cell labelled as "$\text{Cell}_a^{G_i}$" can achieve free intra-group interference within the whole subband $f_{B_1} = \{f_{B_{1,1}}, \ldots, f_{B_{1,N}}\}$ under network MIMO systems. However, subbands f_{B_2} and f_{B_3} are still affected by two first-tier cells and five second-tier cells. We therefore define f_{B_1} as the primary band of $\text{Cell}_a^{G_i}$ for group G_i. Similarly, we define f_{B_2} and f_{B_3} as the primary band of $\text{Cell}_b^{G_i}$ and $\text{Cell}_c^{G_i}$, respectively. Therefore, the cell users served by different subbands among a group can have different signal quality. Note that this service fairness issue is different from the unbalanced signal quality issue mentioned in Section V-C.

The service fairness issue can be resolved by the proposed regrouping and partner selection scheme. Assume that cell 0 is grouped with cells 4 and 5 with primary band f_{B_1} at certain time slot one, as shown in Fig. 5. Cell 0 will regroup with cells 1 and 6 at the next time slot two by counterclockwise rotating way to reselect coordinated partner. After this regroup, the primary band of cell 0 becomes f_{B_2}. Similarly, cell 0 regroups with cells 2 and 3 at time slot three by counterclockwise reselecting coordinated partner again and the corresponding primary band becomes f_{B_3}. In this way, all cells will simultaneously "rotate" and regroup with two new neighboring cells at a new time slot, where "rotate" means the coordinated partner reselection procedure. Take the three cells $\{0, 4, 5\}$ an example. Those cells form a group at time slot one. At time slot two, cell 0's regroup set is now $\{1, 0, 6\}$, cell 4's regroup set is $\{3, 12, 4\}$, and cell 5's regroup set is $\{5, 14, 15\}$. Similarly, cell 0's regroup becomes $\{2, 3, 0\}$, cell 4's regroup set is $\{4, 13, 14\}$, and cell 5's regroup set is $\{6, 5, 16\}$ at time slot three. Each cell has the chance to cooperate with neighboring six cells in order and each sector has the opportunity to become the primary band under this kind of time-division multiple access (TDMA) based regrouping and partner selection scheme. Similar concept can be also applied to frequency-division multiple access (FDMA) manner by further partitioning each outer subband f_{B_p} into three disjoint subsets. Then each subset of f_{B_p} regroups with different neighboring cells.

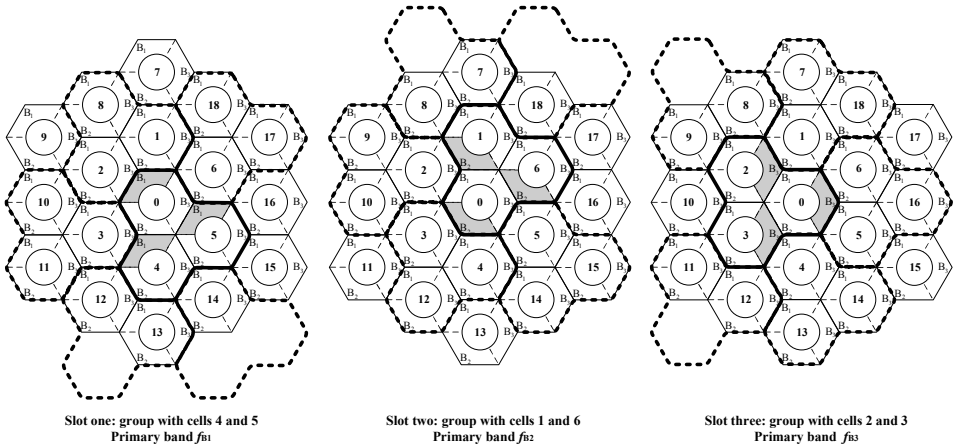

Fig. 5. Example of cells regrouping and partner selection for cell 0.

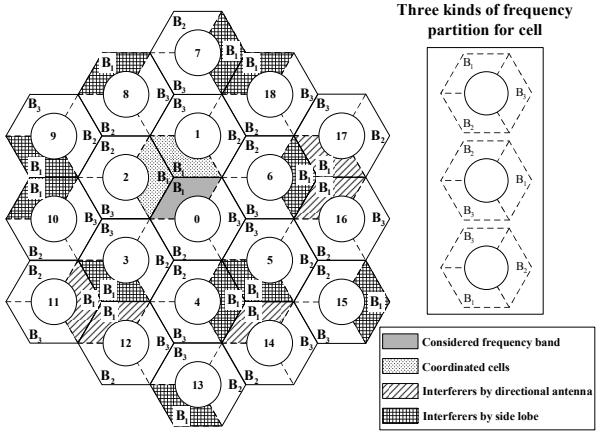

Fig. 6. Interference example for 3-cell FFR-based network MIMO with rearranged tri-sector frequency partition (consider cell 0).

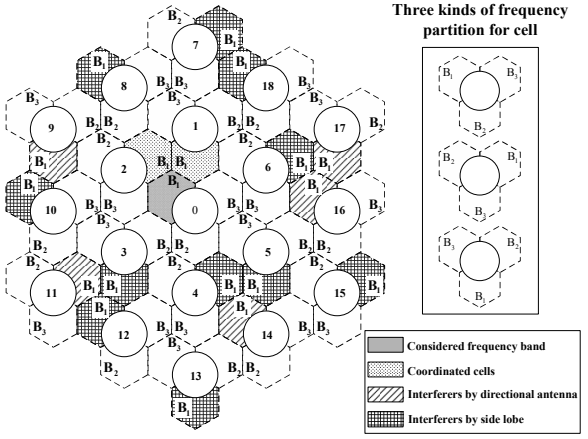

Fig. 7. Interference example for 3-cell FFR-based network MIMO with rearranged tri-sector frequency partition and 60° cell sectoring (consider cell 0).

C. FFR-based Network MIMO with Rearranged Tri-Sector Frequency Partition

1) Cell Planning for 120-degree Tri-Sector Architecture: In this section, we propose another multi-cellular architecture with rearranged tri-sector frequency partitions among cells. As shown in Fig. 6, there are totally three kinds of frequency partitions. After this rearranged tri-sector frequency partition among a multi-cellular system, a cell coordinates with six neighboring cells to form three individually network MIMO groups for each subband. For example, cell 0 coordinates with cells 1 and 2 for subband f_{B_1}, with cells 3 and 4 for subband f_{B_2}, and with cells 5 and 6 for subband f_{B_3}. In other words, we perform 3-cell network MIMO transmission in each subband.

From Fig. 6, when a user of cell 0 utilizes one of RU $f_{B_{1,n}}$ $(n = 1, \ldots, N)$ in frequency band f_{B_1}, the interference sources are cells {1, 2, 11, 12, 14, 16, 17} under the assumption of perfect 120° sector antenna. Similarly we use the network MIMO technique to cancel the two most severe interfering sources. That is, the two first-tier interference from cells 1 and 2 (the dotted area in Fig. 6). The channel matrix for the group $\{0, 1, 2\}$ in $f_{B_{1,n}}$ is

$$\mathbf{H}(f_{B_{1,n}}) = \begin{bmatrix} h_{(0),0} & h_{(0),1} & h_{(0),2} \\ h_{(1),0} & h_{(1),1} & h_{(1),2} \\ h_{(2),0} & h_{(2),1} & h_{(2),2} \end{bmatrix} . \tag{18}$$

For the users in cell 0, we now eliminate the interference caused by $h_{(0),1}$ and $h_{(0),2}$ (from cells 1 and 2) by network MIMO through a small-sized (3×3) matrix computation. Ideally, there are only five second-tier interferers for each subband. Similar the network MIMO with regular tri-sector frequency partition, this cooperation can also be applied to all cells not only for a particular cooperated group. However, there is no service fairness issue for network MIMO systems with rearranged tri-sector frequency partition. As a result, we avoid cells regrouping to ease the complexity in deploying the network MIMO.

2) Cell Planning for 60-degree Tri-Sector Architecture: To address the effects of cell planning with different sectorization techniques, we further design the 3-cell network MIMO systems with three 60° cell sectoring. Here we consider rearranged tri-sector frequency partition to avoid the

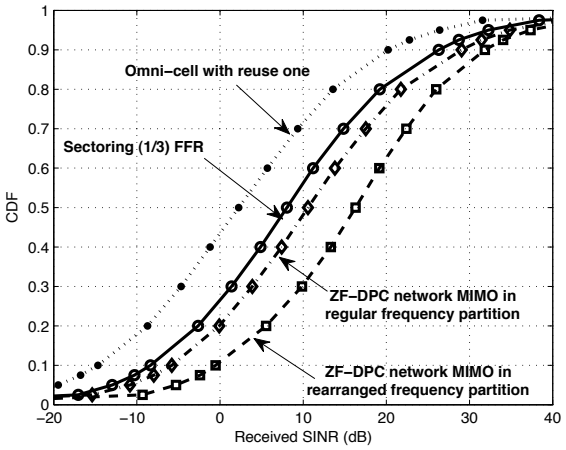

Fig. 8. Comparison of received SINR for conventional 120° tri-sector (1/3) FFR cellular systems and 3-cell ZF-DPC network MIMO systems with regular and rearranged tri-sector frequency partitions.

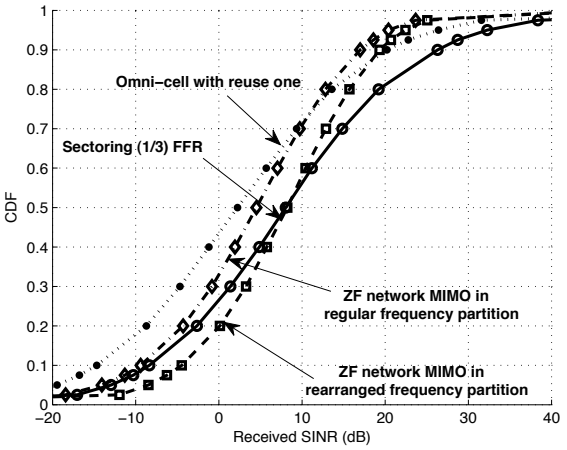

Fig. 9. Comparison of received SINR for conventional 120° tri-sector (1/3) FFR cellular systems and 3-cell ZF network MIMO systems with regular and rearranged tri-sector frequency partitions.

cells regrouping procedure. Figure 7 shows the example of the proposed rearranged 60° tri-sector network MIMO systems. In this design, each cell has three hexagon-shaped sectors with different frequency assignment. The cells with 60° and 120° sectors are also called as the clover-leaf-shaped cells and diamond-shaped cells, respectively [16], [17]. Generally, this clover-leaf-shaped cells can match sector contour better than the cells with diamond-shaped sectors [16]. Additionally, the cells with 60° sectoring can use spectrum more efficiently [17]. Similar to the case of 120° sectoring, each cell under 60° sectoring performs three individually 3-cell network MIMO coordinations with its six neighboring cells for each frequency partition. The two first-tier interferers (the dotted area in Fig. 7) are cancelled through network MIMO transmissions. The 3-cell coordination structure can also be implemented for all the cells.

D. Complexity Comparison of Regular and Rearranged Frequency Partitions

With the assumption of perfect sector directional antennas, the regular tri-sector frequency partition leads to a simpler channel matrix than the rearranged tri-sector frequency partition, e.g. (17) versus (18). For QR decomposition used for ZF-DPC network MIMO, an $m \times n$ ($m \geq n$) matrix $\mathbf{A}$ needs $2n^2(m - n/3)$ flops by the Householder QR algorithm [41], where one flop is a complex multiplication or an addition floating-point operation. The simplified channel matrix for regular frequency partition is an upper Hessenberge matrix and can be factorized by the Givens Hessenberg QR algorithm with $3n^2$ flops, where an $n \times n$ matrix $\mathbf{A}$ is called the upper Hessenberg matrix if entry $a_{i,j} = 0$ whenever $i > j+1$. As a result, the complexity of constructing weight matrix utilizing ZF-DPC network MIMO transmissions for the regular and rearranged frequency partitions are $3M^2$ flops and $\frac{4}{3}M^3$ flops respectively, where $M = 3$ in our considered 3-cell network MIMO architecture. For an $n \times n$ channel inverse operation used for ZF network MIMO, we need LU factorization with $\frac{2}{3}n^3$ flops by Gaussian elimination [41]. For the upper Hessenberg matrix, the LU factorization can be completed with n^2 flops. The complexity between the regular and rearranged frequency partitions are M^2 flops and $\frac{2}{3}M^3$ flops, respectively.

Note that the computational savings of the regular tri-sector frequency partition compared to the rearranged tri-sector frequency partition is under the assumption of using perfect sector directional antennas to construct the simplified channel matrix (17). For actual antenna pattern, the channel matrix of the regular tri-sector frequency partition will not be zero elements due to the effects of imperfect radiation from the sidelobe and backlobe, i.e., $h_{(4),0}$, $h_{(5),0}$, $h_{(5),4}$, $h_{(4),5} \neq 0$ in (17). As a result, both regular and rearranged tri-sector frequency partitions perform full 3×3 matrix computations with the same computational complexity.

Another advantage of the rearranged tri-sector frequency partition over the regular sector frequency partition is service fairness described in Section VI-B1. If network MIMO is employed at the regular tri-sector frequency partition, we need extra cell regrouping procedures to ensure the service fairness among the coordinated cells in each group.

Finally, we summarize the features of the proposed FFR-based 3-cell network MIMO systems: (i) using a small coordination size $M = 3$ to perform low complexity network MIMO systems, (ii) reducing the effects of IGI via the combination of FFR and directional antennas, (iii) avoiding the unbalanced signal quality issue caused by larger coordination size M. Note that actual cell sectorization cannot be perfect by using directional antenna pattern (1). The other cells will also affect the received signal quality of cell 0. However, by taking advantage of sectoring and FFR, the impact caused by the side-lobe and back-lobe transmissions (the grid areas in Fig. 4, Fig. 6 and Fig. 7) is not significant compared to the omni-cell with universal frequency reuse factor of one.

VII. Numerical Results

In this section, we show the SINR performances of the proposed FFR-based 3-cell network MIMO systems. Consider

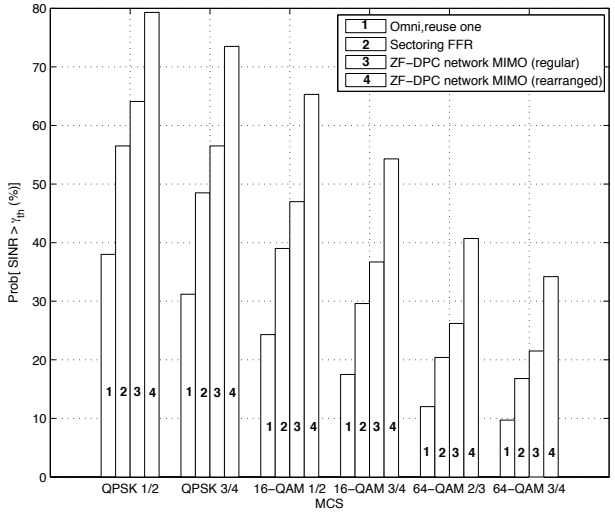

Fig. 10. The percentage of mobile's SINR above the requirements of different MCSs under FFR-based 3-cell ZF-DPC network MIMO. The data rate are {10, 15, 20, 30, 40, 45} Mbits/s for different MCSs {QPSK$\frac{1}{2}$, QPSK$\frac{3}{4}$, 16-QAM$\frac{1}{2}$, 16-QAM$\frac{3}{4}$, 64-QAM$\frac{2}{3}$, 64-QAM$\frac{3}{4}$} under $BW = 10$ MHz.

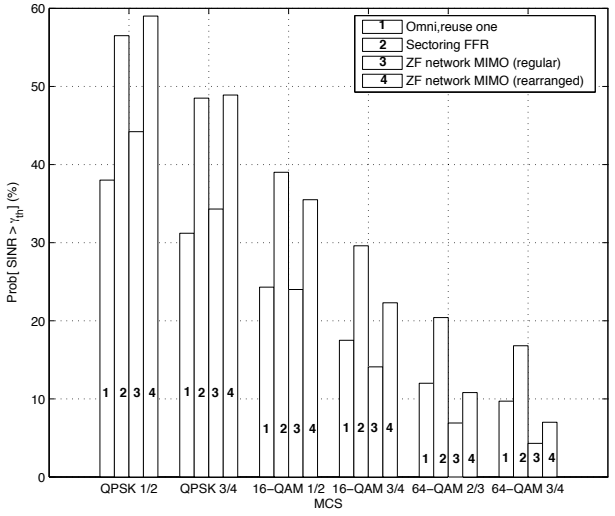

Fig. 11. The percentage of mobile's SINR above the requirements of different MCSs under FFR-based 3-cell ZF network MIMO. The data rate are {10, 15, 20, 30, 40, 45} Mbits/s for different MCSs {QPSK$\frac{1}{2}$, QPSK$\frac{3}{4}$, 16-QAM$\frac{1}{2}$, 16-QAM$\frac{3}{4}$, 64-QAM$\frac{2}{3}$, 64-QAM$\frac{3}{4}$} under $BW = 10$ MHz.

a multi-cellular system with BS-to-BS distance $R_{\text{B2B}} = 2$ km. The interference-free SNR at cell edge is $\Gamma = 18$ dB for 120° sectorized cells. The same values of BS-to-BS distance and Γ (for same transmission power comparison) are used for the clover-leaf-shaped cells. The standard deviation of shadowing is 8 dB and the path loss exponent $\mu = 4$. Mobile users are uniformly distributed within each sector/cell. The channel response between any user-and-cell pair is represented by (3), where the angle-depend antenna pattern is considered. In this paper, we assume perfect CSI obtained at each BS and a synchronized backhaul connection between the coordinated BSs to execute network MIMO transmissions. We leave the effects of imperfect CSI and synchronization delay as the future work. We did not consider the effect of inner region here and set the inner distance be zero. In the next section, we will discuss how to design the uncoordinated inner region for FFR-based multi-cellular broadband system.

A. Effects of Frequency Planning among Coordinated Cells

At first, we present the received SINR performance for 3-cell coordination with both regular and rearranged tri-sector frequency partitions. The performance of network MIMO with ZF-DPC and ZF transmissions are shown in Figs. 8 and 9, respectively. The cell planning is 120° sectoring. The results of the omni-cells with universal frequency reuse factor of one (black point legend) and sectoring 1/3 FFR layout (circle legend) are also presented for comparisons, where 1/3 means reuse factor = 1, but three sector per cell and each sector has different band under the regular tri-sector frequency partition.

From Fig. 8, we find that the gain of interfering sources reduction (from 18 reduce to 7) by sectoring 1/3 FFR is quite significant which is about 10 dB improvement at the 90-th percentile of the received SINR. With the help of 3-cell ZF-DPC network MIMO, the SINR can be further improved especially for the proposed rearranged tri-sector frequency partition scenario. For example, at the 90-th percentile of the received SINR, there are 2.7 dB and 8.5 dB improvements for the regular and rearranged scenario, respectively.

Fig. 9 shows the jointly effects of FFR and 3-cell ZF-based network MIMO. The gain of the ZF-based network MIMO is actually lower than that of the traditional 1/3 FFR-based cellular system with the regular tri-sector frequency partition. After applying the rearranged scenario, the performance gain is also not significant. It is because the actual average power of data stream becomes smaller according to (11). Even if no first-tier interference exist through coordination, the signal quality of the ZF-based network MIMO system is lower than that of the ZF-DPC network MIMO system.

One important issue for system operators is how many users can be supported for a specific data rate. This performance metric can be quantified by the help of the coverage probability or the reliability function defined as

$$P(\gamma_{th}) \triangleq \text{Prob}[\text{SINR} > \gamma_{th}] \ . \tag{19}$$

Figures 10 and 11 shows the values $P(\gamma_{th})$ in percentage for different MCS levels. From Fig. 10, the system can support higher percentage of users with different MCSs transmission under the proposed joint FFR and ZF-DPC network MIMO scheme, especially for the rearranged tri-sector frequency partition method. For example, there are about $5.5 \sim 8$ % and $15 \sim 26$ % gains over the case for the FFR system with sectoring. Nevertheless, in Fig. 11, one can observe that the ZF-based network MIMO system in both rearranged and regular tri-sector frequency partition schemes may perform worse than the pure sectoring FFR without network MIMO when 16-QAM or higher modulation levels are considered. This phenomenon can be explained by the fact that the ZF weights in (11) may decrease the transmit average data stream power.

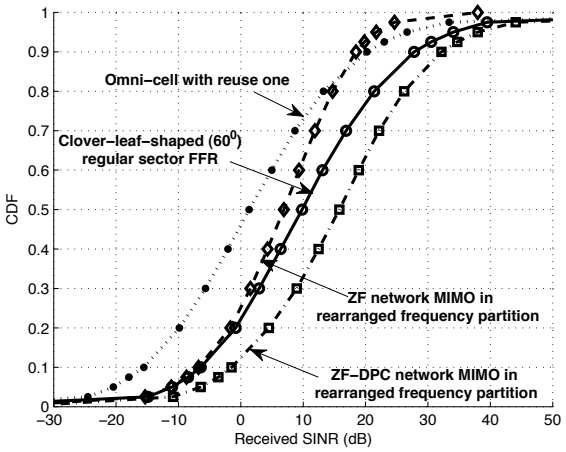

Fig. 12. The CDFs of received SINR for omni-cell with reuse factor of one, 60° regular tri-sector (1/3) FFR cellular systems and proposed rearranged partition-based 3-cell network MIMO systems in 60° cell sectoring.

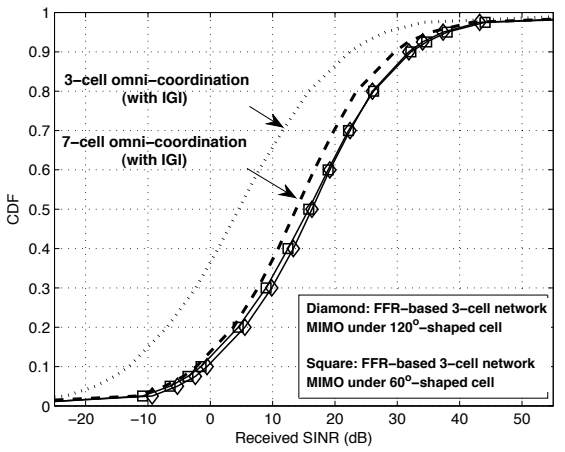

Fig. 13. Performance comparison of proposed FFR-based 3-cell network MIMO with general omni-directional 3-cell and 7-cell network MIMO systems.

B. Effects of Cell Planning with Various Sectorizations

Secondly, we consider the effect of cell planning with different sector directional antenna setups. Figure 12 shows the received SINR performance with 60° sectorized cell planning. We find that the advantage of pure using regular sectorization is obvious under 60° cell sectoring. It is because cell with 60° sectoring can perform better than 120° sectoring [16] [17]. When further applying 3-cell network MIMO, the ZF-DPC can obtain similar SINR performance compared with 120° sectorized cells. However, the gain of ZF-based network MIMO scheme is not very significant at the 90-th percentile of the received SINR, and is actually lower than that by using tri-sector FFR scheme. In other words, under the rearranged tri-sector frequency partition, the proposed 3-cell network MIMO enhances the signal quality more effectively on cell planning with 120° tri-sector architecture than with 60° tri-sector architecture. Note that the performance of the omni-cells with universal frequency reuse factor of one is different in Fig. 8 and Fig. 9 due to different cell planning although the difference is not much.

C. Benefit of Joint Frequency Partition and Network MIMO

Finally, we show the potential gains of combining tri-sector FFR and network MIMO in Fig. 13. Take ZF-DPC as the example. The performance degradations caused by IGI for the 3-cell and 7-cell network MIMO systems are significant. However, taking advantage of joint tri-sector FFR and network MIMO, the proposed FFR-based 3-cell network MIMO architecture (for both cell sectorizations) with rearranged tri-sector frequency partition can even outperform conventional 7-cell network MIMO system. The improvement is about 2 dB for 60° sectoring and 3 dB for 120° sectoring at 90-th percentile of the received SINR. It shows the potential benefit of using a small number of coordinated cells.

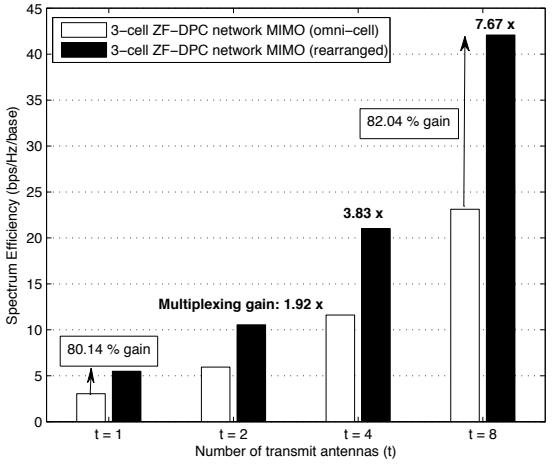

Fig. 14. Comparison of spectrum efficiency of the proposed rearranged three-cell network MIMO and the conventional omni-directional three-cell network MIMO system for various numbers of sector antennas at each base station.

D. Benefits of Network MIMO with Multiple Antennas at Each Base Station

In future wireless broadband systems, BS may equip multiple antennas for exploring performance gains from transmit diversity or spatial multiplexing techniques. In this section, we consider the scenario that t transmit antennas are equipped at each sector to serve t individual users with one single receive antenna. The dimension of the channel matrix for the M-cell network MIMO systems becomes $tM \times tM$ with the transmitted signal vector

$$\mathbf{x} = \mathbf{W}\mathbf{s} = \begin{bmatrix} w_{1,1} & \cdots & w_{1,tM} \\ \vdots & \ddots & \vdots \\ \underbrace{w_{M,1}}_{\triangleq \mathbf{w}_1} & \cdots & \underbrace{w_{tM,tM}}_{\triangleq \mathbf{w}_{tM}} \end{bmatrix} \begin{bmatrix} s_1 \\ \vdots \\ s_{tM} \end{bmatrix}. \quad (20)$$

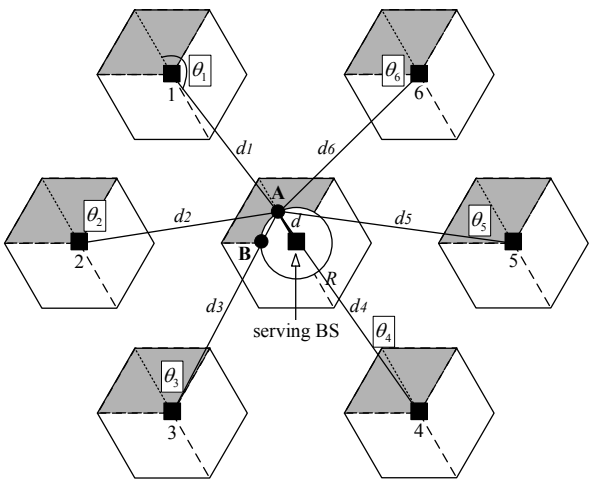

Fig. 15. The considered interference scenario for examining the uncoordinated inner distance (region).

With equal BS power P_{BS}, the constraint in (9) becomes (21) by uniform transmit power in each sector/cell BS.

$$\begin{bmatrix} |w_{1,1}|^2 & \cdots & |w_{1,M}|^2 \\ \vdots & \ddots & \vdots \\ |w_{tM,1}|^2 & \cdots & |w_{tM,tM}|^2 \end{bmatrix} \begin{bmatrix} p_1 \\ \vdots \\ p_{tM} \end{bmatrix} \leq \frac{P_{\text{BS}}}{t} \mathbf{1}_{tM} \quad . \tag{21}$$

Figure 14 shows the spectrum efficiency versus the number of transmit antennas t for the 3-cell ZF-DPC network MIMO systems with rearranged tri-sector frequency partition and conventional omni-directional cell. Spectrum efficiency is calculated according to the sum rate of t users' achievable capacity. The channel matrix reorder algorithm for the ZF-DPC network MIMO transmission is based on [40]. As t increases, the sum rates of both the omni-cell and rearranged tri-sector setups are improved by almost t times compared to the case with one single antenna at BS. For the 3-cell network MIMO with up to eight antennas per sector, the proposed rearranged tri-sector FFR architecture can obtain about 80% higher spectrum efficiency. However, equipping multiple antennas at BS will increase the complexity for a network MIMO system. For example, the complexity of QR decomposition and channel inverse now become $\frac{4}{3}(tM)^3$ flops and $\frac{2}{3}(tM)^3$ flops, respectively.

VIII. Uncoordinated Inner Region Design

In this section, we design the uncoordinated inner region for tri-sector cell planning based on the worst-case SINR analysis. The benefit of creating an inner region is that the allocated RUs can be more dynamically (uncoordinated) unitized for mobiles within the (usually circle) region than the sectorized outer regions with fixed RUs. In addition, although the considered coordination size $M = 3$ is a small value, the complexity of employing network MIMO schemes over all frequency RUs will become a burden for the system operator. To find an uncoordinated region on top of the tri-sector cell planning with reasonable signal quality is hence an important task for broadband network MIMO systems.

We focus on the 120° sectoring cell with regular and rearranged tri-sector frequency partitions. We analyze the worst-case SINR by ignoring the effects of shadowing and fast fading. By (4) and (5) (omitted index k and j), we have

$$\begin{aligned} \gamma &= \frac{A(\theta)\left(\frac{d}{d_{\text{ref}}}\right)^{-\mu}\Gamma}{1+\sum_{i\in\mathcal{I}} A(\theta_i)\left(\frac{d_i}{d_{\text{ref}}}\right)^{-\mu}\Gamma} \\ &= \left[\frac{1}{A(\theta)\Gamma}\left(\frac{d_{\text{ref}}}{d}\right)^{-\mu} + \sum_{i\in\mathcal{I}}\left(\frac{A(\theta_i)}{A(\theta)}\right)\left(\frac{d_i}{d}\right)^{-\mu}\right]^{-1} \\ &\overset{(a)}{\approx} \left[\sum_{i\in\mathcal{I}}\left(\frac{A(\theta_i)}{A(\theta)}\right)\left(\frac{d_i}{d}\right)^{-\mu}\right]^{-1} \quad , \end{aligned} \tag{22}$$

where (a) is approximated by the signal-to-interference ratio (S/I). With deterministic parameters d_i and θ_i, we can obtain the distance value d by the mathematical software tool. Because the received signal power from the serving BS and interference power from surrounding cells vary with user's location, we consider the performance at the two extreme locations, i.e., the location **A** and the location **B** as shown in Fig. 15. The former represents the user locating at the main-beam direction of the tri-sector cell which has the maximal antenna gain; the latter represents the user locating at the boundary of the tri-sector cell where the antenna gain is 3 dB lower than the main-beam direction.

Here, we consider two-tier interference so that $\mathcal{I} = \{1, 2, \ldots, 18\}$ in which the number element represents cell index. Denote the cell radius as R ($= d_{\text{ref}}$) and the considered mobile at position **A** with distance d away from the serving BS. The corresponding distances between mobile and interferers are

$$\text{1st-tier cells} \begin{cases} d_1^A = d_2^A = \sqrt{(\sqrt{3}R/2)^2 + (3R/2 - d)^2} \\ d_3^A = d_6^A = \sqrt{(\sqrt{3}R)^2 + d^2} \\ d_4^A = d_5^A = \sqrt{(\sqrt{3}R/2)^2 + (3R/2 + d)^2} \end{cases}$$

$$\text{2nd-tier cells} \begin{cases} d_7^A = d_9^A = \sqrt{(\sqrt{3}R)^2 + (3R - d)^2} \\ d_{10}^A = d_{18}^A = \sqrt{(3\sqrt{3}R/2)^2 + (3R/2 - d)^2} \\ d_{11}^A = d_{17}^A = \sqrt{(2\sqrt{3}R)^2 + d^2} \\ d_{12}^A = d_{16}^A = \sqrt{(3\sqrt{3}R/2)^2 + (3R/2 + d)^2} \\ d_{13}^A = d_{15}^A = \sqrt{(\sqrt{3}R)^2 + (3R + d)^2} \\ d_8^A = 3R - d \\ d_{14}^A = 3R + d \end{cases} . \tag{23}$$

When mobile user locates at the position **A**, the angle between user and serving BS is $\theta^A = 0$, i.e., in the main-beam direction of the sector antenna. Due to different frequency assignments among cells, the co-channel interferers may point to different directions for regular and rearranged tri-sector frequency partitions, resulting in unequal antenna gains (angles). To be distinguishable, we use $\hat{\theta}_i^A$ and $\tilde{\theta}_i^A$ to represent the relative angles with interferer i for regular and rearranged tri-sector frequency partitions, respectively. The details of angles between the mobile and the main-beam direction of interfering BSs are listed in the Appendix.

TABLE I
THE INNER AND UNCOORDINATED DISTANCES d (METERS) FOR REQUIRED SINR.

SINR (dB)	Inner region	Regular (at **A**)	Regular (at **B**)	Rearranged (at **A**)	Rearranged (at **B**)
6	761 m	1139 m	867 m	797 m	816 m
8.5	678 m	1021 m	774 m	716 m	721 m
11.5	584 m	879 m	669 m	626 m	620 m
15	489 m	723 m	557 m	532 m	517 m
19	395 m	571 m	447 m	437 m	418 m
21	355 m	507 m	400 m	395 m	376 m

Similarly, as a mobile locates at position **B** with distance d to the serving BS, the corresponding distances between the mobile and interferers are

$$\text{1st-tier cells}\begin{cases} d_1^B = d_4^B = \sqrt{(\sqrt{3}R)^2 + d^2} \\ d_2^B = d_3^B = \sqrt{(\sqrt{3}R/2)^2 + (3R/2 - d)^2} \\ d_5^B = d_6^B = \sqrt{(\sqrt{3}R/2)^2 + (3R/2 + d)^2} \end{cases}$$

$$\text{2nd-tier cells}\begin{cases} d_7^B = d_{13}^B = \sqrt{(2\sqrt{3}R)^2 + d^2} \\ d_8^B = d_{12}^B = \sqrt{(3\sqrt{3}R/2)^2 + (3R/2 - d)^2} \\ d_9^B = d_{11}^B = \sqrt{(\sqrt{3}R)^2 + (3R - d)^2} \\ d_{14}^B = d_{18}^B = \sqrt{(3\sqrt{3}R/2)^2 + (3R/2 + d)^2} \\ d_{15}^B = d_{17}^B = \sqrt{(\sqrt{3}R)^2 + (3R + d)^2} \\ d_{10}^B = 3R - d \\ d_{16}^B = 3R + d \end{cases} \quad (24)$$

The corresponding angles between the mobile and the interfering BSs are also listed in the Appendix.

For examining the inner region (distance) with omni-directional antenna, we can use above analysis by setting $A(\theta_i) = 1$. In this case, a mobile has the same SINR quality at both position **A** and **B**. In other words, the omni-directional antenna produces a circle region with radius d for equal signal quality.

Table I shows the inner and uncoordinated distances corresponding to different SINR requirements with both regular and rearranged tri-sector frequency partitions. We find that the cells with regular frequency partitions can extend a larger distance as mobile locates close to the main-beam direction of a sector antenna (**A**) than to the sector edge (**B**). The SINR guaranteed distances are also larger than that of a tri-sector FFR cell planning which further partitions an inner region by omni-directional antenna. Oppositely, the cells with rearranged tri-sector frequency partitions has similar distance extensions as mobile locates close to the main-beam direction or to the sector edge. This is because there are two face-to-face interferers in the rearranged scenario. When a mobile locates in the main-beam direction of a sector antenna, the interference also come from the main-beam directions. Additionally, the extended distances in both **A** and **B** are close to the values of the omni-inner region. That is, the contour of uncoordinated region by rearranged tri-sector frequency partition will be close to the region by omni-directional antenna. As a result, we have the following comments:

- If cell planning combined with rearranged tri-sector frequency partition, we can construct the inner region with assigning suitable spectrum for uncoordinated transmissions. In the outer region, we can use network MIMO scheme to further improve the SINR.
- If cell planning combined with regular frequency partition, it may not be easy to establish the inner region for tri-sector FFR cellular system. Mobiles out of the uncoordinated distance can use network MIMO. However, the improvements are not significant according to the discussion in Section VII

IX. CONCLUSIONS

In the paper, from the aspects of architecture and deployment, we have presented a FFR-based 3-cell network MIMO tri-sector base station architecture that can effectively overcome the inter-group interference and relieve the burden of executing the complex multi-BS joint processing for a huge number of cluster of cells. We further proposed a rearranged tri-sector frequency partition to exploit the interference mitigation capability of the network MIMO transmission. We demonstrated that using a 3-cell coordinated network MIMO with the proposed rearranged tri-sector frequency partition can outperform the 7-cell coordinated network MIMO with omni-directional cell. We also analyzed how to determine the interior region for the FFR-based systems and find that under 120^o sector antenna architecture the proposed tri-sector frequency partition is more feasible for the FFR-based MIMO system than the regular tri-sector frequency partition. This kind of 3-cell coordinated network MIMO architectures are particularly useful because the IEEE 802.16m WiMAX standard body has specified that the default number of neighboring cells in the collaborative MIMO transmission is three.

There are many interesting research directions that can be extended from this work including: (1) to design a low-complexity network MIMO transmission algorithm based on the proposed 3-cell architecture such as codebook-based beamforming adopted in the 3GPP LTE-A and IEEE 802.16m, since the ZF-DPC network MIMO algorithm is still quite complicated; (2) to design the protocols to determine when the network MIMO algorithm should be initiated for the outer region users in the FFR-based network MIMO, and evaluate its performance in a dynamic traffic environment; (3) to evaluate the effects of imperfect CSI on the proposed 3-cell network MIMO architecture.

ACKNOWLEDGEMENT

The authors wish to thank Dr. Jack Winters for his insightful discussion and valulable suggestions on the study of joint network MIMO and frequency reuse techniques.

APPENDIX

When mobile locates at the position **A**, the details of angles between the mobile and the main-beam direction of interfering BSs are

$$\begin{aligned}
&I_1, I_2 : \hat{\theta}_i^A = \tan^{-1}\left(\frac{3R-2d}{\sqrt{3}R}\right) + \frac{\pi}{2};\\
&I_3, I_6 : \hat{\theta}_i^A = \frac{\pi}{2} - \tan^{-1}\left(\frac{d}{\sqrt{3}R}\right);\\
&I_4, I_5 : \hat{\theta}_i^A = \frac{\pi}{2} - \tan^{-1}\left(\frac{3R+2d}{\sqrt{3}R}\right);\\
&I_7, I_9 : \hat{\theta}_i^A = \pi - \tan^{-1}\left(\frac{\sqrt{3}R}{3R-d}\right);\\
&I_{10}, I_{18} : \hat{\theta}_i^A = \pi - \tan^{-1}\left(\frac{3\sqrt{3}R}{3R-2d}\right);\\
&I_{11}, I_{17} : \hat{\theta}_i^A = \frac{\pi}{2} - \tan^{-1}\left(\frac{d}{2\sqrt{3}R}\right);\\
&I_{12}, I_{16} : \hat{\theta}_i^A = \tan^{-1}\left(\frac{3\sqrt{3}R}{3R+2d}\right);\\
&I_{13}, I_{15} : \hat{\theta}_i^A = \tan^{-1}\left(\frac{\sqrt{3}R}{3R+D}\right);\\
&I_8 : \hat{\theta}_i^A = \pi; \qquad I_{14} : \hat{\theta}_i^A = 0\ ,
\end{aligned} \tag{25}$$

for regular tri-sector frequency partition, and

$$\begin{aligned}
&I_1, I_2 : \tilde{\theta}_i^A = \tan^{-1}\left(\frac{3R-2d}{\sqrt{3}R}\right) - \frac{\pi}{6};\\
&I_3, I_6 : \tilde{\theta}_i^A = \frac{2\pi}{3} + \tan^{-1}\left(\frac{d}{\sqrt{3}R}\right);\\
&I_4, I_5 : \tilde{\theta}_i^A = \frac{\pi}{6} + \tan^{-1}\left(\frac{3R+2d}{\sqrt{3}R}\right);\\
&I_7, I_9 : \tilde{\theta}_i^A = \frac{\pi}{3} + \tan^{-1}\left(\frac{\sqrt{3}R}{3R-d}\right);\\
&I_{10}, I_{18} : \tilde{\theta}_i^A = \hat{\theta}_i^A = \pi - \tan^{-1}\left(\frac{3\sqrt{3}R}{3R-2d}\right);\\
&I_{11}, I_{17} : \tilde{\theta}_i^A = \frac{\pi}{6} + \tan^{-1}\left(\frac{d}{2\sqrt{3}R}\right);\\
&I_{12}, I_{16} : \tilde{\theta}_i^A = \hat{\theta}_i^A = \tan^{-1}\left(\frac{3\sqrt{3}R}{3R+2d}\right);\\
&I_{13}, I_{15} : \tilde{\theta}_i^A = \frac{\pi}{3} + \tan^{-1}\left(\frac{\sqrt{3}R}{3R+D}\right);\\
&I_8 : \tilde{\theta}_i^A = \hat{\theta}_i^A = \pi; \qquad I_{14} : \tilde{\theta}_i^A = \hat{\theta}_i^A = 0\ ,
\end{aligned} \tag{26}$$

for rearranged tri-sector frequency partition.

When mobile locates on **B**, with regular tri-sector frequency partition, the angles related to the first-tier interfering BSs are

$$\begin{aligned}
&I_1 : \hat{\theta}_i^B = \frac{\pi}{3} + \tan^{-1}\left(\frac{\sqrt{3}R}{d}\right);\\
&I_2 : \hat{\theta}_i^B = \frac{2\pi}{3} + \tan^{-1}\left(\frac{\sqrt{3}R}{3R-2d}\right);\\
&I_3 : \hat{\theta}_i^B = \frac{\pi}{6} + \tan^{-1}\left(\frac{3R-2d}{\sqrt{3}R}\right);\\
&I_4 : \hat{\theta}_i^B = \frac{\pi}{6} - \tan^{-1}\left(\frac{d}{\sqrt{3}R}\right);\\
&I_5 : \hat{\theta}_i^B = \frac{\pi}{3} - \tan^{-1}\left(\frac{\sqrt{3}R}{3R+2d}\right);\\
&I_6 : \hat{\theta}_i^B = \frac{\pi}{3} + \tan^{-1}\left(\frac{\sqrt{3}R}{3R+2d}\right)\ ,
\end{aligned} \tag{27}$$

and the angles corresponding to the second-tier interfering BSs are

$$\begin{aligned}
&I_7 : \hat{\theta}_i^B = \frac{\pi}{3} + \tan^{-1}\left(\frac{2\sqrt{3}R}{d}\right);\\
&I_8 : \hat{\theta}_i^B = \frac{5\pi}{6} + \tan^{-1}\left(\frac{3R-2d}{3\sqrt{3}R}\right);\\
&I_9 : \hat{\theta}_i^B = \frac{2\pi}{3} + \tan^{-1}\left(\frac{\sqrt{3}R}{3R-d}\right);\\
&I_{10} : \hat{\theta}_i^B = \frac{2\pi}{3};\\
&I_{11} : \hat{\theta}_i^B = \frac{2\pi}{3} - \tan^{-1}\left(\frac{\sqrt{3}R}{3R-d}\right);\\
&I_{12} : \hat{\theta}_i^B = \frac{\pi}{6} + \tan^{-1}\left(\frac{3R-2d}{3\sqrt{3}R}\right);\\
&I_{13} : \hat{\theta}_i^B = \frac{\pi}{6} - \tan^{-1}\left(\frac{d}{2\sqrt{3}R}\right);\\
&I_{14} : \hat{\theta}_i^B = \frac{\pi}{3} - \tan^{-1}\left(\frac{3\sqrt{3}R}{3R+2d}\right);\\
&I_{15} : \hat{\theta}_i^B = \frac{\pi}{3} - \tan^{-1}\left(\frac{\sqrt{3}R}{3R+d}\right);\\
&I_{16} : \hat{\theta}_i^B = \frac{\pi}{3};\\
&I_{17} : \hat{\theta}_i^B = \frac{\pi}{3} + \tan^{-1}\left(\frac{\sqrt{3}R}{3R+d}\right);\\
&I_{18} : \hat{\theta}_i^B = \frac{\pi}{3} + \tan^{-1}\left(\frac{3\sqrt{3}R}{3R+2d}\right)\ .
\end{aligned} \tag{28}$$

Similarly, with rearranged tri-sector frequency partition, the angles for the worst case position **B** related to the first-tier

and second-tier interfering BSs are

$$
\begin{aligned}
I_1 &: \tilde{\theta}_i^B = \frac{\pi}{6} - \tan^{-1}\left(\frac{d}{\sqrt{3}R}\right); \\
I_2 &: \tilde{\theta}_i^B = \tan^{-1}\left(\frac{\sqrt{3}R}{3R-2d}\right); \\
I_3 &: \tilde{\theta}_i^B = \frac{2\pi}{3} + \tan^{-1}\left(\frac{\sqrt{3}R}{3R-2d}\right); \\
I_4 &: \tilde{\theta}_i^B = \frac{\pi}{2} + \tan^{-1}\left(\frac{d}{\sqrt{3}R}\right); \\
I_5 &: \tilde{\theta}_i^B = \frac{\pi}{3} + \tan^{-1}\left(\frac{\sqrt{3}R}{3R+2d}\right); \\
I_6 &: \tilde{\theta}_i^B = \frac{\pi}{2} + \tan^{-1}\left(\frac{3R+2d}{\sqrt{3}R}\right), \qquad (29)
\end{aligned}
$$

and

$$
\begin{aligned}
I_7 &: \tilde{\theta}_i^B = \frac{\pi}{2} + \tan^{-1}\left(\frac{d}{2\sqrt{3}R}\right); \\
I_8 &: \tilde{\theta}_i^B = \hat{\theta}_i^B = \frac{5\pi}{6} + \tan^{-1}\left(\frac{3R-2d}{3\sqrt{3}R}\right); \\
I_9 &: \tilde{\theta}_i^B = \frac{\pi}{6} + \tan^{-1}\left(\frac{3R-d}{\sqrt{3}R}\right); \\
I_{10} &: \tilde{\theta}_i^B = \hat{\theta}_i^B = \frac{2\pi}{3}; \\
I_{11} &: \tilde{\theta}_i^B = \tan^{-1}\left(\frac{\sqrt{3}R}{3R-d}\right); \\
I_{12} &: \tilde{\theta}_i^B = \hat{\theta}_i^B = \frac{\pi}{6} + \tan^{-1}\left(\frac{3R-2d}{3\sqrt{3}R}\right); \\
I_{13} &: \tilde{\theta}_i^B = \frac{\pi}{3} + \tan^{-1}\left(\frac{2\sqrt{3}R}{d}\right); \\
I_{14} &: \tilde{\theta}_i^B = \hat{\theta}_i^B = \frac{\pi}{3} - \tan^{-1}\left(\frac{3\sqrt{3}R}{3R+2d}\right); \\
I_{15} &: \tilde{\theta}_i^B = \pi - \tan^{-1}\left(\frac{\sqrt{3}R}{3R+d}\right); \\
I_{16} &: \tilde{\theta}_i^B = \hat{\theta}_i^B = \frac{\pi}{3}; \\
I_{17} &: \tilde{\theta}_i^B = \frac{\pi}{3} - \tan^{-1}\left(\frac{\sqrt{3}R}{3R+d}\right); \\
I_{18} &: \tilde{\theta}_i^B = \hat{\theta}_i^B = \frac{\pi}{3} + \tan^{-1}\left(\frac{3\sqrt{3}R}{3R+2d}\right). \qquad (30)
\end{aligned}
$$

REFERENCES

[1] 3GPP TSG RAN 1 R1-101695. (2010, Feb.) "Text proposal for 3GPP TR 36.814 on CoMP".

[2] 3GPP TR 36.814 v9.0.0. (2010, Mar.) "Evolved universal terrestrial radio access (E-UTRA); further advancements for E-UTRA physical layer aspects (Release 9)".

[3] *IEEE. Standard 802.16. Part 16: air interface for fixed and mobile broadband wireless access systems – DRAFT amendment to IEEE standard for local and metropolitan area networks - advanced air interface*, IEEE P802.16m/D4, Feb. 2010.

[4] M. K. Karakayali, G. J. Foschini, R. A. Valenzuela, and R. D. Yates, "On the maximum common rate achievable in a coordinated network," *IEEE International Conf. of Commun.*, vol. 9, pp. 4333 – 4338, Jun. 2006.

[5] M. K. Karakayali, G. J. Foschini, and R. A. Valenzuela, "Network coordination for spectrally efficient communications in cellular systems," *IEEE Trans. Wireless Commun.*, vol. 13, no. 4, pp. 56 – 61, Aug. 2006.

[6] G. J. Foschini, M. K. Karakayali, and R. A. Valenzuela, "Coordinating multiple antenna cellular networks to achieve enormous spectral efficiency," *IEE Proc. Commun.*, vol. 153, no. 4, pp. 548 – 555, Aug. 2006.

[7] H. Zhang and H. Dai, "Cochannel interference mitigation and cooperative processing in downlink multicell multiuser MIMO networks," *EURASIP Journal on Wireless Commun. and Networking*, pp. 222 – 235, Feb. 2004.

[8] M. Costa, "Writing on dirty paper," *IEEE Trans. Inf. Theory*, vol. 29, no. 3, pp. 439 – 441, May 1983.

[9] G. Caire and S. Shamai, "On the achievable throughput of a multiantenna Gaussian broadcast channel," *IEEE Trans. Inf. Theory*, vol. 49, no. 7, pp. 1691 – 1706, Jul. 2003.

[10] S. Vishwanath, N. Jindal, and A. Goldsmith, "Duality, achievable rates, and sum-rate capacity of gaussian MIMO broadcast channels," *IEEE Trans. Inf. Theory*, vol. 49, no. 10, pp. 2658 – 2668, Oct. 2003.

[11] P. Viswanath and D. Tse, "Sum capacity of the vector Gaussian broadcast channel and uplink-downlink duality," *IEEE Trans. Information Theory*, vol. 49, no. 8, pp. 1912 – 1921, Aug. 2003.

[12] J. Wang and L. B. Milstein, "CDMA overlay situations for microcellular mobile communications," *IEEE Trans. Commun.*, vol. 43, no. 2/3/4, pp. 603 – 614, Feb./Mar./Apr. 1995.

[13] WiMAX Forum. (2006, Aug.) "Mobile WiMAX - Part I: A technical overview and performance evaluation". [Online]. Available: www.wimaxforum.org

[14] IEEE C802.16m-09/0970. (2009, Apr.) "Collaborative zone to support multi-cell MIMO operation in IEEE 802.16m". [Online]. Available: http://www.ieee802.org/16/tgm/contrib/

[15] IEEE C802.16m-09/2280. (2009, Nov.) "Frequency planning for inter-cell interference reduction in 3-cell collaborative MIMO system". [Online]. Available: http://www.ieee802.org/16/tgm/contrib/

[16] L. C. Wang, K. C. Chawla, and L. J. Greenstein, "Performance studies of narrow beam trisector cellular systems," *International Journal of Wireless Information Networks*, vol. 5, no. 2, pp. 89 – 102, Jul. 1998.

[17] L. C. Wang, "A new cellular architecture based on an interleaved cluster concept," *IEEE Trans. Veh. Technol.*, vol. 48, no. 6, pp. 1809 – 1818, Nov. 1999.

[18] L. C. Wang, G. L. Stüber, and C. T. Lea, "Architecture design, frequency planning, and performance analysis for a microcell/macrocell overlaying system." *IEEE Trans. Veh. Technol.*, vol. 46, no. 4, pp. 836 – 848, Nov. 1997.

[19] S. Shamai and B. M. Zaidel, "Enhancing the cellular downlink capacity via co-processing at the transmitting end," *IEEE Veh. Technol. Conf.*, vol. 3, pp. 1745 – 1749, May 2001.

[20] O. Somekh, O. Simeone, Y. Bar-Ness, and A. M. Haimovich, "Distributed multi-cell zero-forcing beamforming in cellular downlink channels," *IEEE Global Telecommun. Conf.*, pp. 1 – 6, Nov. 2006.

[21] A. D. Wyner, "Shannon-theoretic approach to a Gaussian cellular multiple-access channel," *IEEE Trans. Inf. Theory*, vol. 40, pp. 1713 – 1727, Nov. 1997.

[22] S. Jing, D. N. C. Tse, J. Hou, J. B. Spriag, J. E. Smee, and R. Padovani, "Multi-cell downlink capacity with coordinated processing," *Proc. Inform. Theory and Application Workshop*, Jan. 2007.

[23] Y. Liang, A. Goldsmith, G. Foschini, R. Valenzuela, and D. Chizhik, "Evolution of base stations in cellular networks: denser depolyment versus coordination," *IEEE International Conf. of Commun.*, pp. 4128 – 4132, Jan. 2008.

[24] J. Zhang, R. Chen, J. G. Andrews, A. Ghosh, and R. W. Heath, Jr., "Networked MIMO with clustered linear precoding," *IEEE Trans. Wireless Commun.*, vol. 8, no. 4, pp. 1910 – 1921, Apr. 2009.

[25] F. Boccardi and H. Huang, "Limited downlink network coordination in cellular networks," *Proc. IEEE International Symposium Personal, Indoor and Mobile Radio Commun.*, Sep. 2007.

[26] H. Huang, M. Trivellato, A. Hottinen, M. Shafi, P. J. Smith, and R. Valenzuela, "Increasing downlink cellular throughput with limited network MIMO coordination," *IEEE Trans. Wireless Commun.*, vol. 8, no. 6, pp. 2983 – 2989, Jun. 2009.

[27] P. Marsch and G. Fettweis, "A framework for optimizing the uplink performance of distributed antenna systems under a constrained backhaul," *IEEE International Conf. of Commun.*, pp. 975 – 979, Jun. 2007.

[28] ——, "A framework for optimizing the downlink of distributed antenna systems under a constraint backhaul," *Proc. the 13th European Wireless Conf.*, Apr. 2007.

[29] A. Papadogiannis, D. Gesbert, and E. Hardouin, "A dynamic clustering approach in wireless networks with multi-cell cooperative processing," *IEEE International Conf. of Commun.*, pp. 4033 – 4037, May 2008.
[30] S. Venkatesan, "Coordinating base stations for greater uplink spectral efficiency in a cellular network," *Proc. IEEE International Symposium Personal, Indoor and Mobile Radio Commun.*, Sep. 2007.
[31] ——, "Coordinating base stations for greater uplink spectral efficiency: proportionally fair user rates," *Proc. IEEE International Symposium Personal, Indoor and Mobile Radio Commun.*, Sep. 2007.
[32] H. Fujii and H. Yoshino, "Theoretical capacity and outage rate of OFDMA cellular system with fractional frequency reuse," *IEEE Vehicular Technology Conf.*, pp. 1676 – 1680, May 2008.
[33] M. Assaad, "Optimal fractional frequency reuse (FFR) in multicellular OFDMA system," *IEEE Vehicular Technology Conf.*, Sep. 2008.
[34] R. Y. Chang, Z. Tao, J. Zhang, and C. C. J. Kuo, "A graph approach to dynamic fractional frequency reuse (FFR) in multi-cell OFDMA networks," *IEEE International Conf. of Commun.*, Jun. 2009.
[35] F. Khan, *LTE for 4G Mobile Broadband: Air Interface Technologies and Performance*, 1st ed. Cambridge University Press, 2009.
[36] H. Lei, L. Zhang, X. Zhang, and D. Yang, "A novel multi-cell OFDMA system structure using fractional frequency reuse," *Proc. IEEE International Symposium Personal, Indoor and Mobile Radio Commun.*, pp. 1 – 5, Sep. 2007.
[37] C. S. Chiu and C. C. Huang, "Combined partial reuse and soft handover in OFDMA downlink transmission," *IEEE Vehicular Technology Conf.*, pp. 1707 – 1711, May 2008.
[38] H. Huang and R. A. Valenzuela, "Fundamental simulated performance of downlink fixed wireless cellular networks with multiple antennas," *Proc. IEEE International Symposium Personal, Indoor and Mobile Radio Commun.*, vol. 1, pp. 161 – 165, Sep. 2005.
[39] *IEEE. Standard 802.16-2004. Part 16: Air Interface for Fixed and Mobile Broadband Wireless Access Systems – Amendment for Physical and Medium Access Control Layers for Combined Fixed and Mobile Operation in Licensed Bands*, IEEE Std. 802.16-2005, Dec. 2005.
[40] G. Dimić and N. D. Sidiropoulos, "On downlink beamforming with greedy user selection: performance analysis and a simple new algorithm," *IEEE Trans. Signal Process.*, vol. 53, no. 10, pp. 3857 – 3868, Oct. 2005.
[41] G. H. Golub and C. F. V. Loan, *Matrix Computations*, 3rd ed. The Johns Hopkins University Press, 1996.

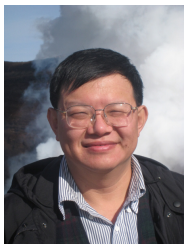

Li-Chun Wang (M'96 – SM'06 – F'11) received the B.S. degree from National Chiao Tung University, Taiwan, R. O. C. in 1986, the M.S. degree from National Taiwan University in 1988, and the Ms. Sci. and Ph. D. degrees from the Georgia Institute of Technology, Atlanta, in 1995, and 1996, respectively, all in electrical engineering.

From 1990 to 1992, he was with the Telecommunications Laboratories of the Ministry of Transportations and Communications in Taiwan (currently the Telecom Labs of Chunghwa Telecom Co.). In 1995, he was affiliated with Bell Northern Research of Northern Telecom, Inc., Richardson, TX. From 1996 to 2000, he was with AT&T Laboratories, where he was a Senior Technical Staff Member in the Wireless Communications Research Department. In August 2000, he became an associate professor in the Department of Electrical Engineering of National Chiao Tung University in Taiwan and has been promoted to the full professor since 2005.

He was elected to the IEEE Fellow grade in 2011 for his contributions in cellular architectures and radio resource management in wireless networks. Dr. Wang was a co-recipient (with Gordon L. Stüber and Chin-Tau Lea) of the 1997 IEEE Jack Neubauer Best Paper Award for his paper "Architecture Design, Frequency Planning, and Performance Analysis for a Microcell/Macrocell Overlaying System," IEEE Transactions on Vehicular Technology, vol. 46, no. 4, pp. 836-848, 1997. He has published over 150 journal and international conference papers. He served as an Associate Editor for the IEEE Trans. on Wireless Communications from 2001 to 2005, the Guest Editor of Special Issue on "Mobile Computing and Networking" for IEEE Journal on Selected Areas in Communications in 2005 and on "Radio Resource Management and Protocol Engineering in Future IEEE Broadband Networks" for IEEE Wireless Communications Magazine in 2006. He is holding nine US patents. His current research interests are in the areas of radio resource management and cross-layer optimization techniques for wireless systems, heterogeneous wireless network design, and cloud computing for mobile applications.

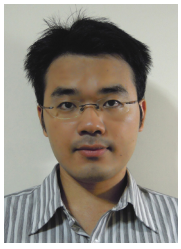

Chu-Jung Yeh (S'08) received the B.S. degree in electrical engineering from National Dong Hwa University, Hualien, Taiwan, in 2004, and the Ph. D. degree in the Institute of Communications Engineering, National Chiao Tung University, Hsinchu, Taiwan. in 2010. He is currently a post doctoral researcher in the Department of Electrical Engineering of National Chiao Tung University. His current research interests include MIMO systems with scheduling, network MIMO systems, and resource management and performance analysis for cellular mobile networks.